Journal of Computational and Applied Mathematics 233 (2010) 2940–2947

Contents lists available at ScienceDirect

Journal of Computational and Applied Mathematics

journal homepage: www.elsevier.com/locate/cam

Numerical conformal mapping of multiply connected domains to regions with circular boundaries

Wei Luo [a], Junfei Dai [a,*], Xianfeng Gu [b], Shing-Tung Yau [c]

[a] Center of Mathematical Sciences, Zhejiang University, China

[b] Computer Science Department, Stony Brook University, NY, USA

[c] Mathematics Department, Harvard University, MA, USA

ARTICLE INFO

Article history:
Received 15 October 2008
Received in revised form 17 November 2009

MSC:
30C30

Keywords:
Numerical conformal mapping
Multiply connected
Circular region

ABSTRACT

We propose a method to map a multiply connected bounded planar region conformally to a bounded region with circular boundaries. The norm of the derivative of such a conformal map satisfies the Laplace equation with a nonlinear Neumann type boundary condition. We analyze the singular behavior at corners of the boundary and separate the major singular part. The remaining smooth part solves a variational problem which is easy to discretize. We use a finite element method and a gradient descent method to find an approximate solution. The conformal map is then constructed from this norm function. We tested our algorithm on a polygonal region and a curvilinear smooth region.

1. Introduction

Surface parametrization is a fundamental problem in computer graphics and computational geometry. Conformal geometry can produce global and canonical parameterizations of surfaces with complicate topology. A multiply connected planar region has many conformally equivalent standard types such as parallel slit regions, circular slit annuli or regions with circular boundary components (called *circular regions*). There is an abundant literature on conformal maps to slit regions, which can usually be described by holomorphic functions satisfying some linear boundary conditions. For example, conformal maps to circular slit regions are considered in [1] and the real part of the logarithm of the mapping function satisfies a Neumann boundary condition. On the other hand, conformal maps to circular regions do not have such simple representations. To find such a map, one way is to represent the inverse map as Laurent series and find the coefficients or other parameters by iterations: [2] used a projection method and [3,4] used a Fornberg-like method. In another approach, [5] solves a Riemann–Hilbert type problem satisfied by the first order approximation of the conformal map in each iteration step. In this paper, we propose a new method to compute the numerical conformal maps to circular regions based on a variational formulation of the problem (4) based on [6]. Due to this variational formulation, the method can be discretized by finite elements. Another advantage is that one can prove the convexity of the functional (Section 3.3) and hence the convergence is good.

The method proposed in this paper has applications in conformal parametrization of a genus 0 surface with boundaries, which is explained in detail in the following sections.

* Corresponding author. Tel.: +86 571 87974078; fax: +86 571 87953035.
E-mail address: jfdai@cms.zju.edu.cn (J. Dai).

0377-0427/$ – see front matter © 2009 Elsevier B.V. All rights reserved.
doi:10.1016/j.cam.2009.11.038

2. Theory

First consider a multiply connected bounded planar region Ω_a, whose boundary components are smooth curves. Ω_a is conformally equivalent to a circular region Ω_c determined up to Möbius transformations. Let $f : \Omega_a \to \Omega_c$ be the conformal map and set $u = \log|f'(z)|$, then u is harmonic in Ω_a and satisfies the boundary condition [6]

$$\frac{\partial u}{\partial n} = -\chi(s) - 2\pi r_v^{-1} e^u, \tag{1}$$

where n is the outer normal vector, $\chi(s)$ is the curvature of $\partial\Omega_a$ with arc length parameter s, r_v is the radius of corresponding circular boundary of Ω_c, depending on which boundary s is on.

In the case that the domain boundary has corners, say a region Ω_p with polygonal boundaries, (1) holds with $\chi(s)$ a multiple of the delta function at each corner,

$$\chi(s) = \beta \cdot \delta(s),$$

where β is the supplement of the corner angle. The delta function will create large errors in a numerical computation. To deal with this, notice that the boundary near a corner consists of two straight lines intersecting at some angle, so the conformal map locally looks like

$$f(z) = f_1((z - z_0)^\alpha),$$

where z_0 is the position of the corner point, $\alpha = \pi/(\pi - \beta)$ and f_1 is some analytic function univalent at 0. So we have

$$\log|f'(z)| = (\alpha - 1)\log|z - z_0| + \text{smooth terms}.$$

Thus u has a logarithmic singularity at the corner. If we subtract from u all the singular parts at corners, the remainder is a harmonic function smooth on boundary. For technical reasons, noting that $(z - z_0)^{\alpha-1}$ might be a multi-valued function over Ω_p, we instead use the following single-valued function on Ω_p which has the same singular part at the corner:

$$\left(\frac{z - z_0}{z - z_0^*}\right)^{\alpha-1}, \tag{2}$$

where z_0^* is some point such that the line segment $z_0 z_0^*$ is outside Ω_p except at z_0. Cancel singularities at all corners $\{z_i\}$ to get a remainder function w, harmonic in Ω_p and smooth to the boundary:

$$u = \sum_i (\alpha_i - 1)(\log|z - z_i| - \log|z - z_i^*|) + w. \tag{3}$$

The normal derivative $(\partial/\partial n)\log|z - z_i|$ vanishes at the two edges of the polygonal boundary adjacent to z_i and is continuous on other edges, while $(\partial/\partial n)\log|z - z_i^*|$ is continuous on the whole boundary. Therefore

$$g(z) := \sum_i (\alpha_i - 1)\frac{\partial}{\partial n}(\log|z - z_i| - \log|z - z_i^*|)$$

is a piecewise continuous function on the boundary. The harmonic function w then satisfies boundary condition

$$\frac{\partial}{\partial n} w = -g(z) - 2\pi r_v^{-1} e^u.$$

As in [6], a solution to above equation is the minimizer of a functional $\Phi(w)$, defined as

$$\Phi(w) := \tfrac{1}{2}\iint_{\Omega_p} \|\nabla w\|^2 + \int_{\partial\Omega_p} g w + 2\pi \sum_v \log \int_{C_v} |G| e^w, \tag{4}$$

where C_v denotes an interior boundary component of Ω_a and

$$G(z) = \prod_i \left(\frac{z - z_i}{z - z_i^*}\right)^{\alpha_i - 1}. \tag{5}$$

Once the harmonic function w is obtained, solving the Cauchy–Riemann equation

$$w_x = w_y^c, \qquad w_y = -w_x^c$$

would produce its harmonic conjugate part w^c. Notice that $G(z)$ is an analytic function such that $\log|G(z)|$ is the sum of singular parts that we subtract from u in (3). Thus $f'(z) = \exp(w + iw^c)G(z)$ is analytic and integration of $f'(z)$ gives the conformal map $f(z)$.

The conformal map f is determined up to a Möbius transformation. This ambiguity can be resolved by fixing images of three points p_i, $i = 1, 2, 3$ on the outer boundary. This leads to a requirement for the unknown w as

$$\int_{p_i}^{p_{i+1}} |G| e^w \, ds = a_i, \quad i = 1, 2, 3, \ (p_4 := p_1), \tag{6}$$

for three fixed positive numbers a_i such that $a_1 + a_2 + a_3 = 2\pi$. (6) fixes the Möbius ambiguity up to rotations and translations of f, which do not affect the shape of the target mesh.

3. Methods and algorithms

3.1. Discretization of the functional

We discretize the problem via a finite element method and look for the minimizer of a discrete version of the functional $\Phi(w)$. The region Ω_a is triangulated into a mesh $\mathcal{T}$ with extra refinement at each corner (if any) as in Fig. 2. Denote the set of nodes, edges, and triangles of $\mathcal{T}$ as V, E, F, respectively. We discretize the unknown function w as a piecewise linear function over $\mathcal{T}$, which is determined by its values on nodes.

The quadratic term of (4) is discretized via the cotangent formula:

$$\frac{1}{2}\sum_{e\in E}(\cot(\beta_1(e))+\cot(\beta_2(e)))(w(t(e))-w(s(e)))^2, \tag{7}$$

where $\beta_1(e)$, $\beta_2(e)$ are the two angles opposite to an edge e in the two triangles containing e; $s(e)$ and $t(e)$ are two end points of e.

The second term of (4), $\int_{\partial\Omega_p} g\,w$, is discretized as

$$\sum_{e\in E}\frac{w(s(e))+w(t(e))}{2}\int_e g(x)\mathrm{d}x.$$

The reason that the integral of $g(x)$ is kept accurate is because one has a closed form of this integral as shown in the next formula. Contribution of an edge e to the weights of its two end points is

$$\frac{1}{2}\int_e g\,\mathrm{d}s=\frac{1}{2}\int_e\frac{\partial}{\partial n}\log|G|\,\mathrm{d}s=\frac{1}{2}\int_e\frac{\partial}{\partial s}\arg G\,\mathrm{d}s=\frac{1}{2}(\arg G(t(e))-\arg G(s(e))). \tag{8}$$

The third term of (4) is the summation of logarithms of scaled lengths of inner boundary components. The scaled length is discretized as a weighted summation of $\exp(w)$. The total scaling at each node is $|f'(z)| = |G(z)|\cdot|\mathrm{e}^w|$. We use the trapezoidal rule for a non-corner node p. Denote

$$\mu(p) := |G(p)|\cdot(l(e_1)+l(e_2))/2,$$

where $l(e_1)$, $l(e_2)$ denote the lengths of two boundary edges adjacent to p. On the other hand, we treat a corner vertex z_i by approximately working out the improper integral of

$$|f'(z)| = |G_1(z)\cdot(z-z_i)^{\alpha_i-1}\cdot\mathrm{e}^{w(z_i)}|, \tag{9}$$

where $G_1(z) = G(z)/(z-z_i)^{\alpha_i-1}$ is some smooth function nonzero at z_i. We approximate the integral by substituting $G_1(z)$ with $G_1(z_i)$ and get

$$\mu(z_i) := \frac{|G_1(z_i)|}{\alpha_i}\left[\left(\frac{l(e_1)}{2}\right)^{\alpha_i}+\left(\frac{l(e_2)}{2}\right)^{\alpha_i}\right]. \tag{10}$$

The numerical scaled length of a boundary component C_v is then

$$l(C_v) := \sum_{p\in V\cap C_v}\mu(p)\cdot\mathrm{e}^{w(p)}, \tag{11}$$

and the third term of (4) is numerically

$$2\pi\sum_v\log l(C_v), \tag{12}$$

where v runs over all inner boundary components.

To fix the Möbius transformation ambiguity, we use a discrete version of (6):

$$\sum_{p\in C_i'}\mu(p)\cdot\mathrm{e}^{w(p)}=a_i,\quad i=1,2,3, \tag{13}$$

where C_i' are the set of nodes on the outer boundary between points p_i and p_{i+1}.

3.2. Elimination of interior variables

Write the $w=(w_i, w_e)$, w_i as the interior node part, w_e as the boundary node part. The discrete functional is then

$$\Phi_D(w)=\frac{1}{2}w^t\mathbf{A}w+\lambda^t\cdot w_e+2\pi\sum_v\log\left[\sum_{p\in C_v}\mu(p)\cdot\mathrm{e}^{w_e(p)}\right], \tag{14}$$

where $\mathbf{A}$ comes from (7), λ comes from (8).

We found that the interior unknown w_i only appears in the quadratic term. Split the matrix $\mathbf{A}$ into block form according to interior node part and boundary node part:

$$\mathbf{A} = \begin{bmatrix} \mathbf{A}_{ii} & \mathbf{A}_{ie} \\ \mathbf{A}_{ei} & \mathbf{A}_{ee}. \end{bmatrix}$$

The functional now reads

$$\frac{1}{2} w_i^t \mathbf{A}_{ii} w_i + w_e^t \mathbf{A}_{ei} w_i + F(w_e),$$

where $F(w_e)$ are terms that depend only on boundary unknowns. A necessary condition that the above functional reaches a minimal point is

$$w_i = -\mathbf{A}_{ii}^{-1} \mathbf{A}_{ie} w_e. \tag{15}$$

Substitute (15) into (14), eliminate w_i and get a minimizing problem for w_e

$$\Phi_D(w_e) = \frac{1}{2} w_e^t \mathbf{A}' w_e + \lambda^t \cdot w_e + 2\pi \sum_v \log\left[\sum_{p \in C_v} \mu(p) \cdot \mathrm{e}^{w_e(p)}\right]. \tag{16}$$

3.3. Convexity of the functional

The quadratic term in (14) comes from (7), which is basically a summation of the square norm of the piecewise constant gradient vector field ∇w, multiplied by the area of each triangle. Hence it is semi-positive definite. The kernel of $\mathbf{A}$ is one dimensional, which corresponds to constant functions. The same properties hold for the quadratic term in (16). Hence this term is a convex function of w_e. The linear term $\lambda^t \cdot w_e$ is also obviously convex. Next, we prove the convexity of the third term in (14).

Take any $p > 1$, $1/p + 1/q = 1$, Holder's Inequality reads

$$\sum a_i b_i \le \left(\sum a_i^p\right)^{1/p} \left(\sum b_i^q\right)^{1/q}$$

for positive $\{a_i\}$, $\{b_i\}$. Apply for

$$a_i = (\mu(i)\mathrm{e}^{w_e(i)})^{1/p}, \qquad b_i = (\mu(i)\mathrm{e}^{w_e'(i)})^{1/q},$$

where i runs over all nodes on a boundary component. We get

$$\sum_i \mu(i)\mathrm{e}^{\frac{1}{p}w_e(i) + \frac{1}{q}w_e'(i)} \le \sum_i (\mu(i)\mathrm{e}^{w_e(i)})^{1/p} (\mu(i)\mathrm{e}^{w_e'(i)})^{1/q}$$

or taking logarithm of above to finish proof of convexity of the third term in (16).

3.4. Gradient descent

A simple gradient descent method is used to find a minimizer of the functional (16). To fix the Möbius transformation ambiguity, we modify the gradient vector by projecting to the tangent space determined by the constraint Eq. (13). The minimizing sequence is altered with a small step size in the modified gradient direction each time.

We use a fixed step size h of the gradient descent method. A good step size is related to the Hessian matrix of the functional (16). For our practical examples, we found that $h = 0.05$ guaranteed convergence of $\Phi_D(w)$ with an error about the size of $1e - 13$ before oscillation around the minimal point.

3.5. Treatment afterwards

Find the harmonic conjugate of w: A minimizer w of (14) approximately solves (4), whose solution is the smooth part of $\log|f'(z)|$. A conjugate harmonic function of w then approximates the smooth part of $\arg f'(z)$. We solve for a conjugate harmonic function w^c via discretization of

$$\min_{w^c} \iint_{\Omega_p} \|\nabla w^c - J\nabla w\|^2 \,\mathrm{d}x\mathrm{d}y,$$

where

$$J\left(\frac{\partial}{\partial x}\right) = \frac{\partial}{\partial y}, \qquad J\left(\frac{\partial}{\partial y}\right) = -\frac{\partial}{\partial x} \tag{17}$$

is the $\pi/2$ counterclockwise rotation of vectors. We discretize w^c also as a piecewise linear function determined by its values at nodes of the triangulation. Similar to deriving the cotangent formula, computation shows that w^c minimizes

$$\sum_{\text{faces}} \sum_{i=1}^{3} \frac{\cot(\beta_i)}{2} (w_{i+2}^c - w_{i+1}^c)^2 + \frac{w_i^c (w_{i+2} - w_{i+1})}{2}, \tag{18}$$

where summation of i is for the three vertices of each triangle element, index counted cyclicly, w_i^c, w_i denote the value at corresponding vertices. We omitted terms depending only on w in (18) since this does not affect the solution of w^c.

Write vector $\tilde{w}$ as

$$\tilde{w}_i = \sum_{i,j,k \text{ on same triangle}} (w_j - w_k)/2,$$

where summation is taken over all node pair j, k adjacent to i such that i, j, k are counterclockwise. Straightforward computation shows that a solution of (18) is

$$w^c = \mathbf{A}^{-1}\tilde{w} + \text{constant}. \tag{19}$$

Find f: The major singular part G in (5) multiplied by $\exp(w + iw^c)$ gives an approximation of the analytic function $f'(z)$. We solve for $f(z)$ by minimizing a discrete version of functional

$$\iint \|\nabla f - f'\|^2 \mathrm{d}x\mathrm{d}y. \tag{20}$$

Specifically, we compute from approximate values of $f'(z)$ the expected shape of each triangle of the mesh $\mathcal{T}$ under map f.

- If no vertices of the triangle is at a corner of original polygon, write z_i, $i = 1, 2, 3$ for original complex coordinates of three vertices and $\bar{f}' = (f'(z_1) + f'(z_2) + f'(z_3))/3$. Three vertices of the expected target triangle in complex coordinates is then
$$z_1^e = 0, \qquad z_2^e = \bar{f}' \cdot (z_2 - z_1), \qquad z_3^e = \bar{f}' \cdot (z_3 - z_1).$$
- If say z_1 is at a corner, the singular part of $f'(z)$ has a $[(z - z_1)/(z - z_1^*)]^{\alpha_1 - 1}$ part and a part $\check{f}$ nonzero at z_1. Here z_1^*, α_1 are as defined in (2). The expected target triangle is then
$$z_1^e = 0, \qquad z_2^e = \frac{\check{f}(z_1)(z_2 - z_1^*)}{\alpha_1}\left(\frac{z_2 - z_1}{z_2 - z_1^*}\right)^{\alpha_1},$$
$$z_3^e = \frac{\check{f}(z_1)(z_3 - z_1^*)}{\alpha_1}\left(\frac{z_3 - z_1}{z_3 - z_1^*}\right)^{\alpha_1}.$$

Write coordinates of vertices of a triangle in expected shape as (x_i^e, y_i^e), $i = 1, 2, 3$. Contributions of this triangle to the real and imaginary part of discrete version of (20) are respectively

$$\begin{aligned} &\sum_{i=1}^{3} \frac{\cot\beta_i}{2}(x_{i+2} - x_{i+1} - x_{i+2}^e + x_{i+1}^e)^2 \\ &\sum_{i=1}^{3} \frac{\cot\beta_i}{2}(y_{i+2} - y_{i+1} - y_{i+2}^e + y_{i+1}^e)^2. \end{aligned} \tag{21}$$

These two equations can be easily solved by a least square method, while fortunately the coefficient matrix is still $\mathbf{A}$. The final coordinate function x_i, y_i is determined up to two constants, corresponding to a translation.

3.6. Summary of the algorithm

1. Triangulate the region, put extra subdivisions near each corner.
2. Generate $\mathbf{A}$, λ, μ, etc., put $w_e = 0$.
3. Compute the gradient vector δw of Φ_D in (16) at current w_e.
4. Compute scaled outer boundary length weight vectors $\mu_i' = \mu_i . \exp(w_e)$, $i = 1, 2, 3$, where $u.v$ denotes a vector whose components are multiplication of corresponding components of u and v, μ_i comes from (13).
5. Project δw to the orthogonal complement space of span$\{\mu_i'\}$ to get $\delta w'$.
6. Update $w_e = w_e - h * \delta w'$.
7. Compare Φ_D for two w_e's. If the difference is within acceptable tolerance then go to next step, otherwise return to step 3.
8. Complete w_e to w via (15).
9. Compute conjugate harmonic function w^c of w as in (19).
10. Compute exponential $\exp(w + iw^c)$ and multiply by G to get an approximation of f'.
11. Compute positions of the target mesh points as in (21).

4. Results

We tested our algorithm for a polygonal domain with three holes. The original shape is as Fig. 1. We use Ansys 10 to generate the mesh with extra subdivisions around each corner as in Fig. 2. We apply gradient descent method to get a solution of (16). In practice, this part is not time consuming since after interior node variable elimination (15), only boundary

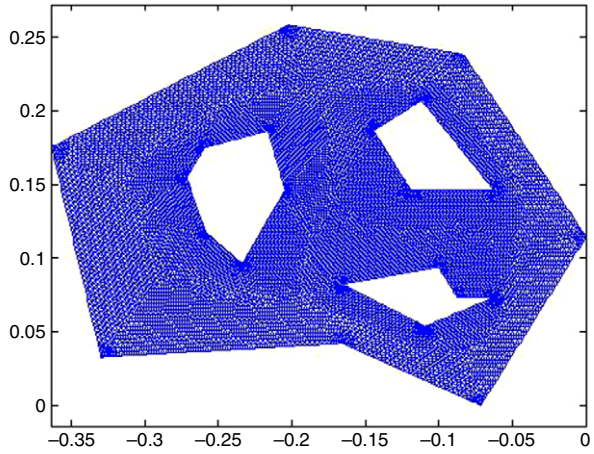

Fig. 1. Original polygonal domain.

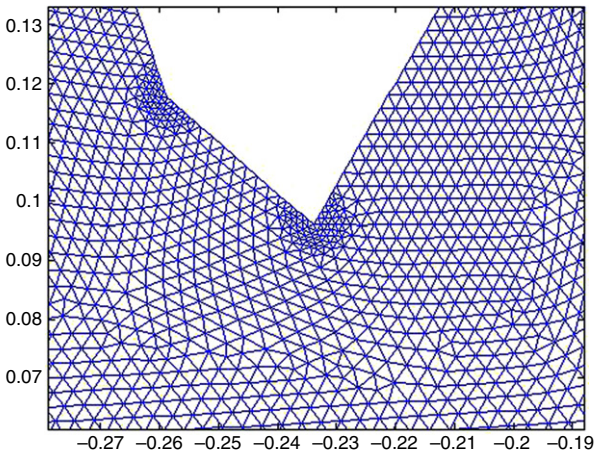

Fig. 2. Extra refinement near a corner.

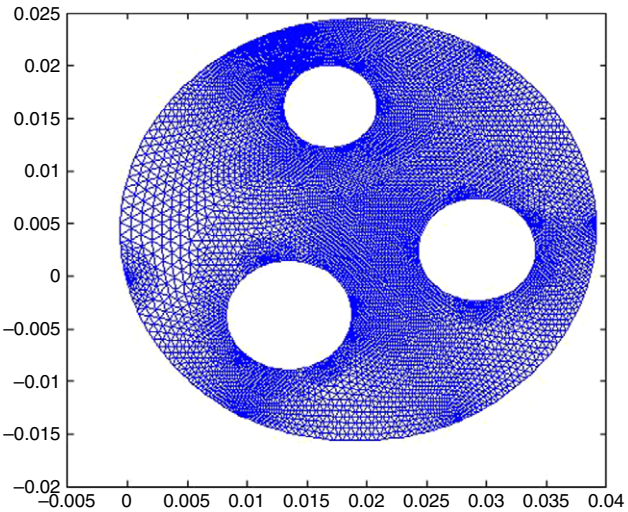

Fig. 3. Target circular region.

unknowns are present. The final shape of the mesh is as Fig. 3 and near a corner as Fig. 4. We compute eccentricity to check whether the boundary components are close to circles. To check whether the map is conformal we compare solutions to the same discrete Dirichlet boundary value problems over two meshes. Each time we put boundary value 1 on one boundary

Table 1
Computational results: rows 1–4 are for Fig. 5, rows 5–12 are for Fig. 1, rows 8–12 are for a triangulation with extra refinement at corners; column 2 of rows 1–8 denote the error of Φ_D when the iteration fails to converge monotonely; eccentricity is measured by the distance of target points of a boundary component to the approximate circle, divided by the radius of the circle; conformality is measured by the difference of solutions to the same Dirichlet boundary value problems over original and target meshes.

# of nodes	Error of $\Phi_D(w_e)$	Boundary eccentricity		Conformality
		Outer (max/ave.)	Inner (max/ave.)	(max/ave.)
102	1.00E−13	0.04/0.01	0.14/0.07	0.02/0.006
389	2.00E−13	0.007/0.002	0.05/0.02	0.007/0.001
1538	1.00E−12	0.002/0.0007	0.01/0.006	0.002/0.0003
5862	1.00E−12	0.0007/0.0002	0.004/0.002	4e−4/7e−5
1262	9.00E−13	0.14/0.04	0.09/0.05	0.03/0.003
3979	2.00E−12	0.07/0.03	0.07/0.03	0.03/0.002
15285	6.00E−12	0.04/0.02	0.04/0.02	0.02/8e−4
9643*	3.00E−12	0.009/0.004	0.01/0.005	0.01/2e−4
9643*	0.1	0.1/0.06	0.01/0.008	0.01/0.002
9643*	0.02	0.04/0.03	0.01/0.003	0.01/8e−4
9643*	0.004	0.02/0.01	0.01/0.004	0.01/5e−4
9643*	2.00E−04	0.01/0.006	0.01/0.005	0.01/2e−4

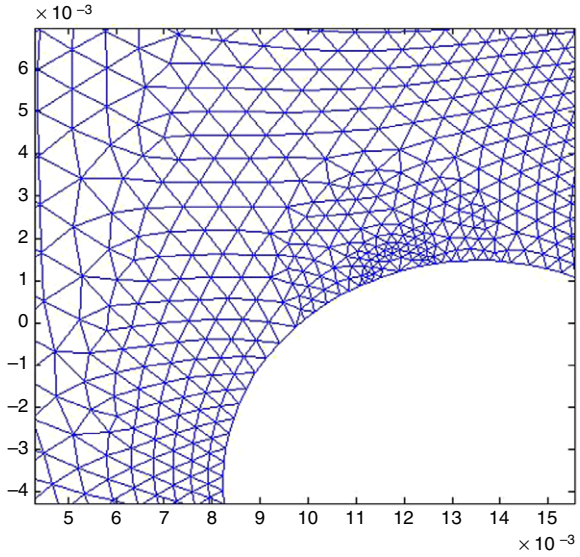

Fig. 4. Target shape of an original corner.

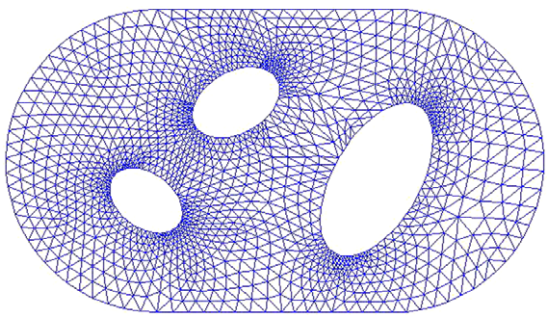

Fig. 5. Original smooth curvilinear domain.

component and 0 on the rest boundary components. From computational results in Table 1 we read that refinement of the mesh near corners significantly improves the roundness of target circles; conformality is not as sensitive as roundness of boundaries to the size of the mesh; inner boundaries converge to nearly circles faster than the outer boundary.

We also tested the method for a domain with curvilinear smooth boundary (Fig. 5). Since this shape is without corners, there is no need to deal with singular parts. The only extra step is to use the nonzero curvature $\chi(s)$ in (1) instead of sum of

delta functions as for polygon boundaries. From results in Table 1 we read that the roundness and conformality of conformal maps for smooth regions are much better than that for polygonal regions, comparing for meshes of similar size; also the conformality improves significantly when the mesh size increases.

5. Discussion

The method used in this paper formulates the conformal mapping problem to multiply connected regions as a variational problem, which behaves well for discretization. One can use other discretization methods, such as using power series to approximate the mapping function. Discretization via series should be less memory consuming and might have more accurate and smoother approximation to the real solution than the piecewise linear approximation in the finite element discretization. Discretization via series depends only on shapes of the boundary component curves. The use of series requires that the whole region should be in a single coordinate patch, i.e., a planar region. On the other hand, finite element discretization would easily generalize to genus 0 surfaces with boundaries. A first thing to consider in such a generalization is to find a local function taking care of the singular part of $\log|f'|$ near a corner point, while in this paper, a global function $(\alpha_i - 1)\log|(z - z_i)/(z - z_i^*)|$ does the job.

The method can be combined with other methods to find conformal parametrization of a genus 0 surface with boundaries. Firstly, glue a disk along each boundary to get a closed surface. Secondly, use the curvature flow method in [7] to find a conformal map to a sphere. Thirdly, use stereographic projection to map the sphere to the plane, with the north pole chosen outside the original surface. Finally, use the method in this paper or any other conformal map method to find a conformal map to a circular region.

For simplicity of programming, we use gradient descent method to find the minimizer of (16). Having proved convexity of the functional, one can consider using Newton's method or BFGS method for a possible better convergence.

Having a approximate f', one can also consider other ways to find the final conformal map f. For example, one can restrict to the class of functions whose images are guaranteed circular.

A more sophisticated way to test the conformality of the final map is as follows: First find the approximate circles of the target boundary components and approximate images of vertices of the domain polygon (not all the vertices of the mesh) on the circles. With this circle and vertex information, use a numerical method of the generalized Schwarz–Christoffel formula in [8] (the generalized Schwarz–Christoffel formula was first derived in [9] for the unbounded case) to map the circular region back to a polygonal region and then compare it to the original polygonal region.

Acknowledgements

The authors thank Zhiqiang Li for kindly providing triangulation data. Wei Luo is supported by the National Natural Science Foundation of China (No. 60503067).

References

[1] Dai Okano, Hidenori Ogata, Kaname Amano, Masaaki Sugihara, Numerical conformal mappings of bounded multiply connected domains by the charge simulation method, Journal of Computational and Applied Mathematics 159 (2003) 109–117.
[2] M.E. Klonowska, W.J. Prosnak, On an effective method for conformal mapping of multiply connected domains, Acta Mechanica 119 (1996) 35–52.
[3] T.K. DeLillo, M.A. Horn, J.A. Pfaltzgraff, Numerical conformal mapping of multiply connected regions by Fornberg-like methods, Numer. Math. 83 (1999) 205–230.
[4] N. Benchama, T.K. DeLillo, T. Hrycak, L. Wang, A simplified Fornberg-like method for the conformal mapping of multiply connected regions—Comparisons and crowding, Journal of Computational and Applied Mathematics 209 (2007) 1–21.
[5] R. Wegmann, Fast conformal mapping of multiply connected regions, Journal of Computational and Applied Mathematics 130 (2001) 119–138.
[6] M. Schiffer, N.S. Hawley, Connections and conformal mapping, Acta Mathematica 107 (1962) 175–274.
[7] Xianfeng Gu, Yalin Wang, Tony F. Chan, Paul M. Thompson, Shing-Tung Yau, Genus zero surface conformal mapping and its application to brain surface mapping, IEEE Transaction on Medical Imaging 23 (8) (2004) 949–958.
[8] Darren Crowdy, The Schwarz–Christoffel mapping to bounded multiply connected polygonal domains, Proc. R. Soc. A 461 (2061) (2005) 2653–2678.
[9] T. DeLillo, A. Elcrat, J. Pfaltzgraff, Schwarz–Christoffel mapping of multiply connected domains, Journal d'Analyse Mathematique 94 (2004) 17–47.